Witnessing the formation and relaxation of dressed quasi-particles in a strongly correlated electron system

Fabio Novelli[1,2], Giulio De Filippis[3], Vittorio Cataudella[3], Martina Esposito[1], Ignacio Vergara[4], Federico Cilento[2], Enrico Sindici[1], Adriano Amaricci[5], Claudio Giannetti[6,7], Dharmalingam Prabhakaran[8], Simon Wall[9], Andrea Perucchi[2,10], Stefano Dal Conte[11], Giulio Cerullo[11], Massimo Capone[5], Andrey Mishchenko[12,13], Markus Grüninger[4], Naoto Nagaosa[12,14], Fulvio Parmigiani[1,2,4] & Daniele Fausti[1,2]

The non-equilibrium approach to correlated electron systems is often based on the paradigm that different degrees of freedom interact on different timescales. In this context, photo-excitation is treated as an impulsive injection of electronic energy that is transferred to other degrees of freedom only at later times. Here, by studying the ultrafast dynamics of quasi-particles in an archetypal strongly correlated charge-transfer insulator ($La_2CuO_{4+\delta}$), we show that the interaction between electrons and bosons manifests itself directly in the photo-excitation processes of a correlated material. With the aid of a general theoretical framework (Hubbard–Holstein Hamiltonian), we reveal that sub-gap excitation pilots the formation of itinerant quasi-particles, which are suddenly dressed by an ultrafast reaction of the bosonic field.

[1] Dipartimento di Fisica, Università degli Studi di Trieste, Via Valerio 2, 34127 Trieste, Italy. [2] Elettra—Sincrotrone Trieste S.C.p.A., 34149 Basovizza, Italy. [3] SPIN-CNR and Dipartimento di Fisica, Università di Napoli Federico II, I-80126 Napoli, Italy. [4] II. Physikalisches Institut, Universität zu Köln, 50937 Köln, Germany. [5] CNR-IOM Democritos National Simulation Center and Scuola Internazionale Superiore di Studi Avanzati (SISSA), Via Bonomea 265, 34136 Trieste, Italy. [6] I-LAMP (Interdisciplinary Laboratories for Advanced Materials Physics), Università Cattolica del Sacro Cuore, I-25121 Brescia, Italy. [7] Department of Physics, Università Cattolica del Sacro Cuore, I-25121 Brescia, Italy. [8] Department of Physics, University of Oxford, Oxford OX1 3PU, UK. [9] ICFO-Institut de Ciencies Fotoniques, Av. Carl Friedrich Gauss, 3, Castelldefels, 08860 Barcelona, Spain. [10] INSTM UdR Trieste-ST, 34149 Basovizza, Italy. [11] IFN-CNR, Dipartimento di Fisica, Politecnico di Milano, Piazza L. da Vinci 32, 20133 Milano, Italy. [12] RIKEN Center for Emergent Matter Science (CEMS), Wako, Saitama 351-0198, Japan. [13] RRC 'Kurchatov Institute', 123182 Moscow, Russia. [14] Department of Applied Physics, University of Tokyo, 7-3-1 Hongo, Bunkyo-ku, Tokyo 113-8656, Japan. Correspondence and requests for materials should be addressed to G.F. (email: giuliode@na.infn.it) or to D.F. (email: daniele.fausti@elettra.eu).

The exotic electronic ground states of transition-metal oxides (TMOs), such as high-temperature superconductivity and colossal magnetoresistance, arise from both the strong interactions among electrons and the complex interplay between the electronic and bosonic degrees of freedom such as lattice vibrations and magnetic excitations[1–4]. A prime example of such complexity is represented by the cuprate family. Starting from parent compounds which are charge-transfer (CT) insulators[5–13], anomalous metallic and eventually high-temperature superconducting phases appear on electron or hole doping[14,15].

The properties of CT insulators are determined by Coulomb repulsion, which forces the electrons to localize, freezing charge fluctuations. In such a state, the coupling between localized fermions and bosonic excitations, which is mediated by charge dynamics, is naively expected to be strongly suppressed[16,17].

Although this scenario is seemingly met when we measure and study the properties of a steady-state Mott insulator, a different situation arises if the system is doped[18–20] or driven out of equilibrium[13,21,22]. In particular, the naive picture would suggest that if we try to excite the system by means of a pulse with photon energy smaller than the CT gap, because of strong electron correlations, we would observe little effect on the material as the localized carriers have no chance to change their state and, therefore, they have no means to couple to bosonic excitations. In our study, a completely different scenario emerges, in which a coupled boson-charge mode is excited leading to an effective renormalization of the CT gap.

Note that in the following we use the general term 'boson'. This is due to the fact that although the Hubbard–Holstein Hamiltonian (HHH) was developed to treat lattice vibrations, the same model can be used to address other kinds of bosonic excitations such as collective electronic modes. The punctual identification of these bosonic modes remains controversial in the cuprates and is beyond the scope of this paper. Further information can be found in refs 23–25. Here, we show that a model including both local Coulomb interaction and coupling with a boson mode (HHH) accounts for our main experimental observations. The effects of the electron–boson coupling are highlighted by comparing the dynamical optical responses of $La_2CuO_{4+\delta}$ driven by pulses with photon energy respectively larger and smaller than the gap, which corresponds to the energy needed to create free charge excitations.

Results

Time-resolved measurements on $La_2CuO_{4+\delta}$. Transient reflectivity experiments on $La_2CuO_{4+\delta}$ were performed with above-gap (~ 3.1 eV) and sub-gap (~ 0.95 eV) ~ 100 fs long pump pulses and broadband probes as detailed in the Methods section. From the measured $\Delta R(\omega, \tau)/R(\omega) = R(\omega, \tau)/R(\omega) - 1$ with $R(\omega, \tau)$, the time-dependent pump-perturbed reflectivity, and $R(\omega)$, the equilibrium reflectivity, we calculate the pump-induced changes of the optical conductivity $\Delta\sigma_1(\omega, \tau) = \sigma_1(\omega, \tau)-\sigma_1(\omega)$ as a function of probe frequency (ω) and pump–probe delay time (τ). Here, $\sigma_1(\omega, \tau)$ and $\sigma_1(\omega)$ are the time-dependent light-perturbed and equilibrium optical conductivity, respectively. The CT peak (CTP) in $\sigma_1(\omega)$ is at ~ 2.3 eV, while the gap, estimated from a simple linear interpolation (red dashed line in Fig. 1), is at about $\Delta = 1.8$ eV for $T = 130$ K and is consistent with previous reports[6–9,26]. The non-vanishing optical conductivity below the gap is due to the presence of tail states. Such tail states originate from the strong interaction between the free charges in excess, coming from oxygen non-stoichiometry[23], and the bosonic degree of freedom[13]. The excess oxygen content $\delta \sim 5 \times 10^{-3}$ is estimated from the measured Néel temperature of

229 K (ref. 27). $\Delta\sigma_1(\omega, \tau)$ is obtained from $\Delta R(\omega, \tau)/R(\omega)$ with a novel data analysis methodology based on the Kramers-Kronig (KK) relations. In short, by knowing the equilibrium reflectivity $R(\omega)$ and the non-equilibrium $\Delta R(\omega, \tau)/R(\omega)$, it is possible to calculate the pump-perturbed reflectivity $R(\omega, \tau)$ and, from it, all the transient optical properties (see Methods).

Temporal response. The results reported in Fig. 2a,b are for pump pulses with photon energy at $E_{pump} = 3.1$ eV and $E_{pump} = 0.95$ eV, respectively, with ~ 0.04 eV pulse bandwidth each (see Methods for details). In the first hundred femtoseconds, we observe striking differences between the photo-excitation with photons at energy $E_{pump} > \Delta$ (Fig. 2a) and $E_{pump} < \Delta$ (Fig. 2b). A smooth rise time (> 100 fs) is detected only for $E_{pump} > \Delta$, while sub-gap excitation leads to a pulse-width-limited rise time of the signal followed by an ultrafast decay. This difference is made evident in Fig. 2c, where the optical response at the CTP is shown as a function of the pump–probe delay. The results in Fig. 2c are normalized to the energy absorbed by the sample for $E_{pump} = 3.1$ eV (solid blue curve) and $E_{pump} = 0.95$ eV (solid red curve), respectively (see Methods for details). Although in a different physical context, it is worth mentioning here that ultrafast responses to an optical pump below the gap in multiple quantum wells[28] and below the electronic excitation energy in molecular systems[29] has been previously reported.

In Fig. 2c, we show that the modifications of the optical response at the CTP induced by the two stimuli are different in the initial dynamics while they become similar for longer delays between the pump and the probe pulses. As the data are normalized to the absorbed energy, the good agreement for large delays indicates that this 'slow' response is directly related to absorption, that is, to real electronic excitations. Such 'slow' response is consistent with previous time-resolved measurements on La_2CuO_4 (refs 30,31), Nd_2CuO_4 (refs 30–32), $YBa_2Cu_3O_y$ (ref. 32) and $Sr_2CuO_2Cl_2$ (ref. 21).

Sub-20 fs pulse experiments. With the aim to resolve the ultrafast rise time observed for $E_{pump} < \Delta$, we performed room temperature ~ 10 fs experiments with $E_{pump} < \Delta$ (1.4 eV with 0.1 eV bandwidth) and $E_{pump} > \Delta$ (2.25 eV with 0.25 eV bandwidth). In spite of the different excitation parameters used for the ~ 10 and ~ 100 fs measurements, we expect the outcome of these experiments to be meaningful for addressing the question concerning the non-thermal ultrafast rise time.

The $\Delta R(\omega, \tau)/R(\omega)$ at $E_{probe} \sim 2.1$ eV is shown in Fig. 2d, while the transient reflectivity spectra at two pump–probe delays are reported in Supplementary Fig. 1 and Fig. 2d. It is evident that also for ~ 10 fs $E_{pump} < \Delta$ pulses the ultrafast shift of the optical response is limited by the temporal resolution of the experiments (Supplementary Fig. 1). Such result sets the upper limit of the timescale of the non-thermal response in $La_2CuO_{4+\delta}$ to 20 fs. Unfortunately, under the present experimental conditions, a direct quantitative comparison of the thermalization times between the ~ 100 and the ~ 10 fs excitations is not meaningful. In particular, the thermalization time is significantly shorter for ~ 10 fs excitations (see Fig. 2c,d). We attribute this effect to the remarkably different conditions in terms of excitation density and spectral content of the pulses used in the experiments (see Methods).

In the following, we will discuss only the spectral responses of the pump–probe data obtained with ~ 100 fs pump pulses where the linear response regime has been proven (see Methods).

Energy-dependent response. We now take advantage of the broadband probe and describe the spectral dependence of the transient response. The energy-dependent $\Delta\sigma_1(\omega, \tau)$ at a
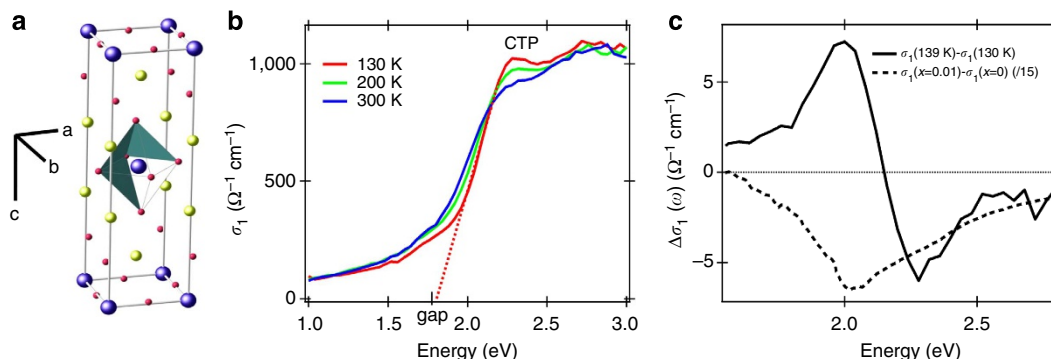
Figure 1 | Equilibrium optical conductivity of lanthanum-copper oxide for polarization in the oxygen plane. (**a**) La_2CuO_4 unit cell with copper in purple, oxygen in red and, lanthanum in yellow. (**b**) In plane optical conductivity at 130 K, 200 K, and room temperature as determined via ellipsometry. The charge-transfer peak (CTP) is indicated. The red dashed straight line allows to define the gap at ~1.8 eV. (**c**) Expected variation of $\sigma_1(\omega)$ on doping (dashed line) or heating (solid line). The solid line is obtained from our ellipsometry data, the dashed line is the difference between the optical conductivity of $La_{1.99}Sr_{0.01}CuO_4$ ($x = 0.01$) and La_2CuO_4 ($x = 0$) at room temperature. This last curve has been calculated starting from the data reported in ref. 6. Specifically, to obtain the $x = 0.01$ doping reported in **c**, we performed a linear interpolation between the $x = 0$ and the $x = 0.02$ spectra shown in ref. 6.
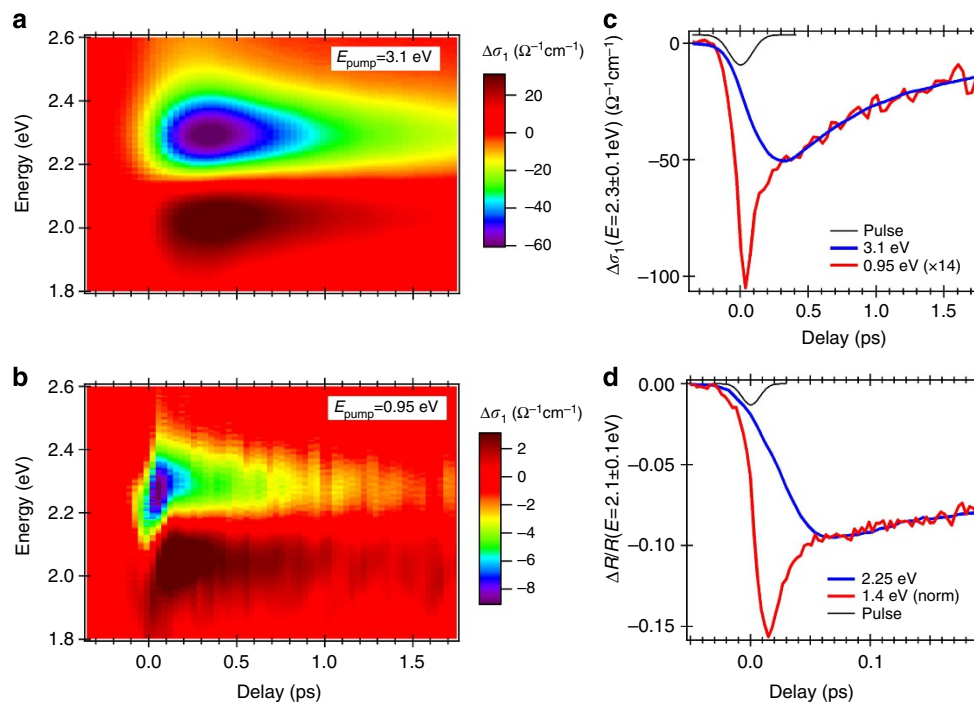

Figure 2 | Time-domain evolution of optical conductivity. The measurements performed at 130 K are reported as a function of probe energy for pump energy (**a**) larger (3.1 eV with 0.04 eV bandwidth) and (**b**) smaller (0.95 eV with 0.04 eV bandwidth) than Δ. (**c**) The transient optical conductivity at $E_{probe} = 2.3$ eV for both pump energies is shown (3.1 eV in blue, 0.95 eV in red). The response for sub-gap excitation is multiplied by the ratio of the absorbed energy densities (see Methods). The black curve depicts the 3.1 eV pump autocorrelation. (**d**) Normalized pump–probe reflectivity measurements performed at room temperature with ~10 fs pulses (in black the pulse duration, see Methods for details).

delay time $\tau = 0.05$ ps averaged over ± 0.05 ps ($\tau = 0.3$ ps, averaged over ± 0.1 ps) is reported in Fig. 3a,b for the two pump energies (blue for 3.1 eV and red for 0.95 eV pulses, respectively).

For $E_{pump} > \Delta$ at both pump–probe delays, we observe a depletion of the optical absorption centred at $E_{probe} \sim 2.3$ eV and an enhanced absorption around $E_{probe} \sim 2.1$ eV. This behaviour can be ascribed to a 'thermal response', that is, it is compatible with the shift towards lower energies of the CTP on heating[27,30,31] as seen in Fig. 1. This is confirmed by comparing the measured $\Delta\sigma_1(\omega, \tau)$ at long pump–probe delays with the expected variation of the equilibrium optical conductivity for a

temperature increase resulting from the pump-induced heating of the sample (black line in Fig. 3b, see Methods for details).

On the contrary, $\Delta\sigma_1(\omega, \tau)$ for $E_{pump} < \Delta$ reveals a significant spectral evolution with time. The main feature remains an optical conductivity depletion around the CTP, but the energy dependence of the response depends on the pump–probe delay time τ. The $\Delta\sigma_1(\omega, \tau)$ has a minimum at $E_{probe} \sim 2.2$ eV within ~100 fs and drifts towards the thermal response only on longer times.

It is important to notice that for $\tau \lesssim 100$ fs and $E_{pump} = 0.95$ eV the optical conductivity displays mainly a negative variation around $E_{probe} \sim 2.2$ eV, which consists of an overall
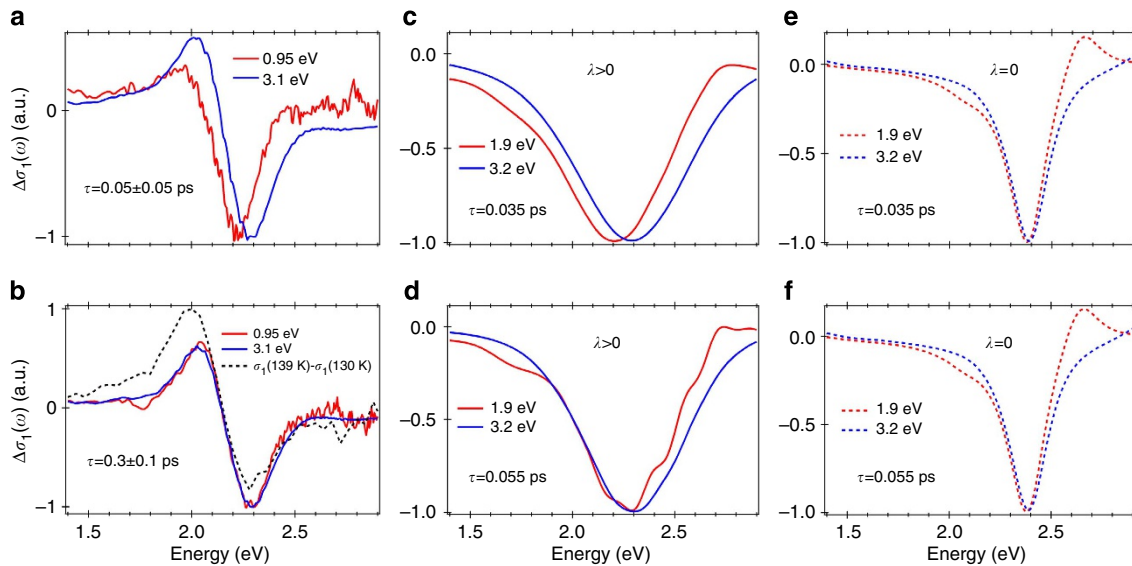
Figure 3 | Experimental and theoretical energy dependence of $\Delta\sigma_1$ at significant pump–probe delays. In **a** and **b**, the experimental data are shown (the pulse bandwidth of about 0.04 eV is omitted in the labels); in **c–f**, the model calculations are reported. In **e** and **f**, the zero-coupling results are reported for comparison. All the graphs share the same energy axis. The data are normalized for the sake of comparison.

non-thermal quench of the CTP. This ultrafast variation of the optical conductivity resembles the one induced by small doping at equilibrium (see the dashed line in Fig. 1b), that is, in both cases a broadband negative response at the CTP is present. To understand these experimental results, we now introduce the HHH.

Discussion

In the one-band Hubbard model, the optical gap for free charge excitations is related to the energy cost for unbound double occupancies (doublons). To explain the differences between the responses to sub-gap and above-gap excitations, one has to consider the two limiting cases predicted by time-dependent perturbation theory: non-adiabatic and adiabatic regimes. The non-adiabatic regime describes real transitions between electronic quantum states where the response is present for some time after the pump pulse is over. On the contrary, in the adiabatic regime the response comes from the deformation of the wave functions by the electric field of the light and the system comes back to the ground state when the pump pulse is over. Taking into account that the system is still out of equilibrium for several picoseconds after the pump pulse is over, we argue that the non-adiabatic contribution with real electronic transitions dominates the experimental response for $E_{pump} > \Delta$ (Fig. 2a). Conversely, both contributions are essential for describing the dynamics for $E_{pump} < \Delta$.

To describe the differences between the responses driven in La$_2$CuO$_{4+\delta}$ by sub-gap ($E_{pump} = 0.95\,eV$) and above-gap ($E_{pump} = 3.1\,eV$) $\sim$100 fs long pump pulses (Fig. 2), we turn to the HHH and introduce the effects of the electromagnetic fields through the classical vector potential $\mathbf{A}(\tau)$ (see Methods). The HHH represents a standard approach for underdoped cuprates where the insulating state arises from the strong repulsion between the electrons. By taking into account both onsite Coulomb repulsion U and an effective electron–boson interaction[30], the HHH can reproduce the equilibrium optical properties of cuprates both undoped and with tiny doping[13] and rationalizes the presence of tail states responsible for the broad below-gap absorption[13,27,33]. We argue that these tail states are responsible for the non-adiabatic contribution for sub-gap pumping and for

the linearity of the optical response as a function of pump fluence (see Methods). Furthermore, we will show that the ultrafast transient optical response observed for $E_{pump} < \Delta$ unveils a mixed regime of light–matter interaction where the light-driven gain of the electron kinetic energy leads to a sudden reaction of the bosonic field. As doping also drives a kinetic energy gain of the carriers, one naively expects an off-equilibrium ultrafast response similar to the one associated to doping at equilibrium (see Figs 1b and 3).

The HHH is given by the sum of three terms:

$$H_t = -t \sum_{i,\mu,\sigma} \left(e^{iA(\tau)} c^{\dagger}_{i+\mu,\sigma} c_{i,\sigma} + \text{H.c.} \right), \quad (1)$$

$$H_U = U \sum_i \left(n_{i,\uparrow} - \frac{1}{2} \right)\left(n_{i,\downarrow} - \frac{1}{2} \right), \quad (2)$$

$$H_{ebi} = \omega_0 \sum_i a^{\dagger}_i a_i + g\omega_0 \sum_i \left(a^{\dagger}_i + a_i \right)(1 - n_i), \quad (3)$$

which account for the kinetic energy of the electrons (equation (1)), the onsite Coulomb repulsion (equation (2)) and the electron–boson interaction (equation (3)), respectively. In equations (1–3), t is the hopping amplitude, $c^{\dagger}_{i,\sigma}$ is the fermionic creation operator, μ is a lattice vector, $a^{\dagger}_i$ creates a boson at site i with frequency ω_0 and n_i is the electron number operator. The units are such that $\hbar = 1$. We choose model parameters typical for the cuprates ($t = 0.3\,eV$, $\omega_0 = 0.2t$, and the electron–boson coupling constant $\lambda = \frac{g^2\omega_0}{4t} = 0.5$). The value of the Hubbard repulsion $U = 10t$ yields low-energy physics very similar to that of the $t - J$ model with $J = 4t^2/U$ (see Methods). Although the exact solution for this Hamiltonian is not available, the time evolution of the many-body wavefunction $|\Psi(\tau)\rangle$ can be obtained in a small two-dimensional lattice (eight sites with periodic boundary conditions) by using an exact diagonalization method (time-dependent Lanczos approach) based on a smart truncation of the boson Hilbert space, which has been proven successful in different systems[34,35]. Spin and charge degrees of freedom are treated exactly within numerical precision. The
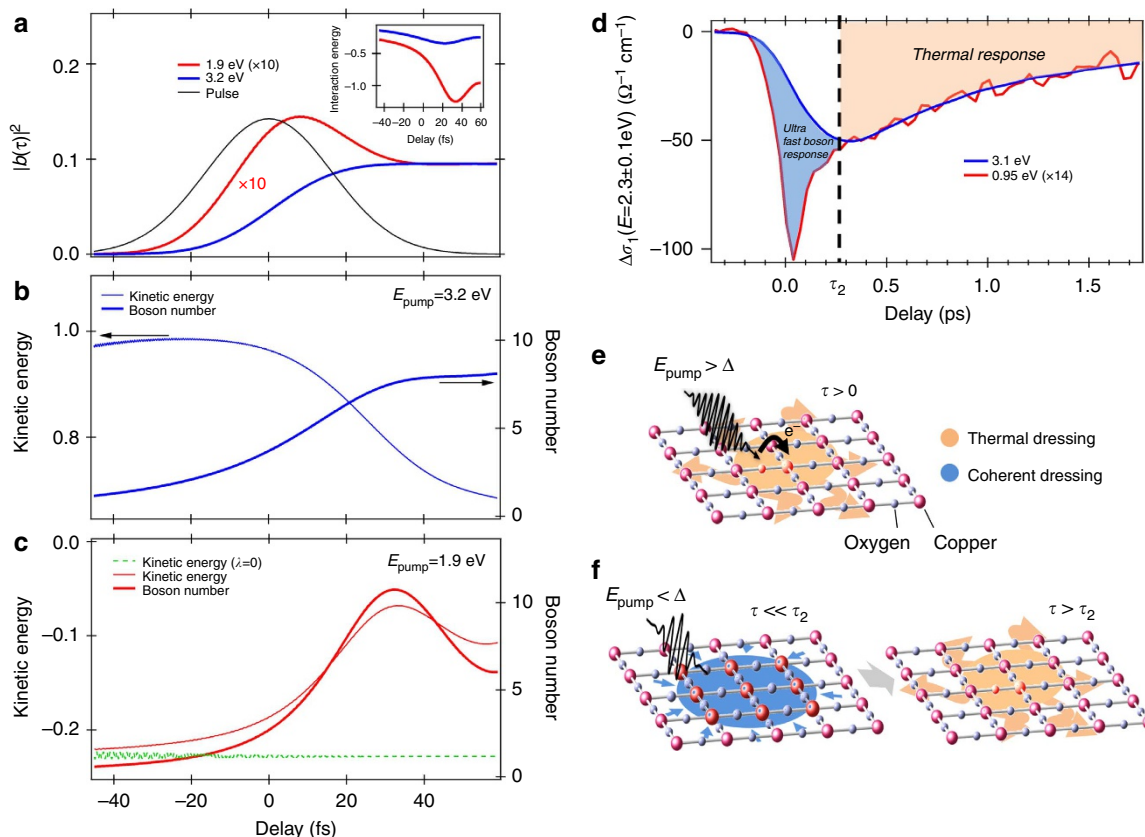
Figure 4 | Hubbard–Holstein calculations. (**a**) The weight, $|b(\tau)|^2$, of the photo-excited component of the wave function as a function of pump–probe delay for excitations below (red) and above (blue) Δ (the sub-gap weight is multiplied by 10.2, that is, it is normalized to that above gap). In the inset of **a**, the interaction energy in eV is shown. The average number of bosons (thick line) and the electron kinetic energy in eV (thin line) for the two excitation wavelengths are reported in **b** and **c**. In **a**, **b** and **c**, the differences between the pump-perturbed quantities and the ground state ones are shown. In **d**, Fig. 2c is reproduced for clarity, with orange and blue shaded areas to underline the slow and fast responses of the bosonic field associated to $E_{pump} > \Delta$ and $E_{pump} < \Delta$, respectively. In **e** and **f**, cartoons of the physical mechanism are sketched. For $E_{pump} > \Delta$ (**e**), the dynamics is consistent with a simple thermalization or 'thermal dressing' scenario; for $E_{pump} < \Delta$ (**f**), the ultrafast drop of kinetic energy goes in pair with the reaction of the bosonic field and a 'coherent dressing' mechanism is in action at very short time delays.

optical conductivity is then calculated for a given value of the pump–probe delay τ, within the linear response theory, starting from the wave-function $|\Psi(\tau)\rangle$ (see Methods for more details).

In Fig. 3c,d we show the calculated $\Delta\sigma_1(\omega, \tau)$ at two different delay times both for above-gap (~ 3.2 eV) and sub-gap (~ 1.9 eV) ~ 40 fs long pump pulses. Please note that the slightly different pulse parameters used in the model compared with the experiment are required by the small lattice adopted in the calculations (see Methods). The major photo-induced feature calculated for $E_{pump} > \Delta$ (Fig. 3c,d) is a reduction of the optical conductivity, which is consistent with the experiments (Fig. 2a and Fig. 3a,b). However, we observe quantitative discrepancies between the calculated linewidths and the measured ones. In particular, the calculated reduction of the optical conductivity extends over a broader energy range. We argue that this is due to the fact that the model is well suited to address doping phenomena[13] but lacks both the detailed crystal structure and a proper thermal reservoir. This interpretation is supported by comparing the expected variation of the optical conductivity on doping[6] (black dashed curve in Fig. 1b) with the model results (Fig. 3b). Hence, for long pump–probe delays or $E_{pump} > \Delta$, the single boson mode contained in the HHH acts as an effective but quantitatively inaccurate thermal bath.

Nonetheless, we stress that the theory accounts for the main experimental features and that a comparison between theory and experiment is fair, as both lie in the linear response regime (see Methods). In particular, both theory and experiments for $E_{pump} < \Delta$ display a spectral response exhibiting an evolution on ultrafast timescales (Fig. 3a–d). We argue that such ultrafast changes of the spectral response are described by the model exclusively in the presence of strong electron–boson interaction, as can be seen by inspection of Fig. 3e,f that are obtained for electron–boson coupling $\lambda = 0$. The ultrafast shift of the optical response for $E_{pump} < \Delta$ may be rationalized as the result of a distortion of the bosonic field around holons and doublons[36,37], leading to an energy renormalization close to the experimentally observed value[13].

In the following we discuss the theoretical results in detail. We separate the wave function $|\Psi(\tau)\rangle = \sqrt{1 - |b(\tau)|^2}|\Psi_{GS}\rangle + b(\tau)|\phi(\tau)\rangle$ into the ground state $|\Psi_{GS}\rangle$ and the photo-excited component $|\phi(\tau)\rangle$, that is, the part of the wavefunction different from the ground state. Here $|b(\tau)|^2$ represents the weight of $|\phi(\tau)\rangle$ in the total wavefunction $|\Psi(\tau)\rangle$. As $|\phi(\tau)\rangle$ includes a doublon–holon pair (see Methods), $|b(\tau)|^2$ is also a rough estimate of the double occupancy density. Indeed, the number of doublons left in the system at $\tau > 0$ is an order of magnitude smaller for $E_{pump} < \Delta$ than for $E_{pump} > \Delta$ (Fig. 4a), confirming that the non-adiabatic processes are less relevant for sub-gap pumping.

To highlight the modifications driven in the system by the pump, we calculate the expectation values of different physical observables in the photo-excited state, that is, $\langle \phi(\tau)|A|\phi(\tau) \rangle$. The operators of interest are the kinetic energy, the number of bosons and the interaction energy. These correspond to the expectation values of H_t (equation (1)), of the first part of H_{ebi} divided by ω_0, and of the second part of H_{ebi} (equation (3)), respectively. These expectation values are related to the ones calculated on the total wavefunction $\langle \Psi(\tau)|A|\Psi(\tau) \rangle$ through the weight $|b(\tau)|^2$ (see Methods for details). The interaction energy carries direct information on the interplay of the bosonic field with the excited charge carriers. Namely, this quantity is proportional to the number of bosons that are accumulated just on the site where doublons or holons are situated.

For $E_{pump} > \Delta$, itinerant doublon–holon pairs are created (Fig. 4a) with a significant kinetic energy during the laser pulse (Fig. 4b). These pairs subsequently relax to lower energies emitting bosons on a longer timescale. The decrease of the average kinetic energy is related to the increase of the average boson number (Fig. 4b). The physics emerging for $E_{pump} > \Delta$ is thus consistent with a thermalization scenario of the photo-excited doublons and holons.

In the case of $E_{pump} < \Delta$, a completely different response is observed. During the pulse, the kinetic energy is negative both for $\lambda = 0$ and for finite λ, but most important is the behaviour immediately after the pulse (Fig. 4c). In case of finite λ, we observe an ultrafast reaction of the bosons, which is apparent both from the maximum of the boson number at $\tau_1 = 35$ fs as well as from the minimum of the interaction energy at the same value of τ (inset of Fig. 4a). Owing to this ultrafast reaction, the kinetic energy increases immediately after the pulse. Altogether, this is a clear signature of the ultrafast formation of strongly dressed quasi-particles. This transient state, leading to the observed optical conductivity drop around the CTP, persists for few tens of femtoseconds and only at longer times evolves into a thermal incoherent state ($\tau_2 > 50$ fs). The time dependence of the kinetic energy and boson number (Fig. 4c) shows that for sub-gap pumping the energy is transferred nearly 'instantaneously' (on a timescale related to the inverse of the boson frequency) from the electromagnetic field into the boson subsystem through the electrons. The comparison of the kinetic energies calculated with and without the electron–boson coupling (solid and dashed lines in Fig. 4c) indicates that the persistence of some dynamics after the end of the pump pulse for $E_{pump} < \Delta$ is possible only with non-vanishing electron–boson interaction. In Fig. 4d we redraw for clarity the data of Fig. 2c, and cartoons of the physical mechanisms described above are shown in Fig. 4e,f for $E_{pump} > \Delta$ and for $E_{pump} < \Delta$, respectively.

The scenario stemming from the exact diagonalization of the Hubbard–Holstein model explains the different response measured for above-gap and sub-gap excitations. In spite of the fact that the model includes only one bosonic field, such field can be excited in a different way by the two excitation schemes. Although for $E_{pump} > \Delta$ the boson field acts as a bath where the excess kinetic electronic energy is deposited after the excitation, sub-gap pumping triggers a quasi-instantaneous distortion of the bosonic field. It is interesting to note that for both theory and experiment the ultrafast response in the optical conductivity for $E_{pump} < \Delta$ gives a transient feature, which is qualitatively analogous to the changes associated to a small doping (Fig. 1c, black dashed curve). This observation leads us towards the speculation that a perturbation with sub-gap photon energy drives a non-thermal tendency to create delocalized strongly dressed quasi-particles. This discloses several possible scenarios where coherent electromagnetic fields can be used to manipulate quantum coherent phases of matter[38,39].

Methods

Experimental details. We performed time-resolved experiments on La$_2$CuO$_{4+\delta}$ by combining broadband probes with ~ 100 fs pump pulses at different wavelengths. To address the pulse-width-limited rise time observed for $E_{pump} < \Delta$, we performed additional measurements with sub-20 fs pulses.

The ~ 100 fs pump pulse measurements were performed with a Ti:Sa amplified laser at 250 kHz repetition rate. The pump energies were tuned to 0.95 eV ($E_{pump} < \Delta$) and to 3.1 eV ($E_{pump} > \Delta$) with durations corresponding to ~ 100 and ~ 140 fs, respectively, and about 0.04 eV bandwidth each. The 0.95 eV pulses are generated with a commercial optical parametric amplifier, the 3.1 eV pulses by second harmonic generation of the fundamental laser light in a 200-μm-thick Beta Barium Borate (BBO) crystal. The broadband probe was generated in a sapphire crystal. As expected for white-light generation[40], the chirp of these probes is mainly linear. Thus, it has been simply corrected with the same straight line for both above-gap (~ 3.1 eV) and sub-gap (~ 0.95 eV) pump pulses. Freshly polished a–b oriented samples were mounted on the cold finger of a helium flow cryostat. The reflectivity changes $\Delta R(\omega, \tau) = R(\omega, \tau)/R(\omega) - 1$ were measured in the 1.5–3.1 eV range at several temperatures between 50 and 330 K. The pump fluences of the measurements shown in Figs 2a–c and 3 are equal to 330 and 170 μJ cm^{-2} for the 3.1 and 0.95 eV pump pulses, respectively. These fluences correspond to about 4×10^{-3} and 1×10^{-3} Ph u^{-1} for $E_{pump} > \Delta$ and $E_{pump} < \Delta$, respectively, where ph u^{-1} stands for photons (ph) absorbed by a chemical unit (u) of La$_2$CuO$_4$. The amplitude of the measured photo-induced variation of the reflectivity is linear with the pump intensity up to two times the excitation densities used in the reported experiments (see Supplementary Fig. 2).

The sub-20 fs measurements were performed with a Ti:Sa amplified source at 1 kHz. The pump energies were tuned to 1.4 eV with 0.15 eV bandwidth ($E_{pump} < \Delta$) and to 2.25 eV with 0.25 eV bandwidth ($E_{pump} > \Delta$) with duration corresponding to ~ 12 and ~ 7 fs, respectively. The short pulses are obtained by compressing the output of a tunable non-collinear optical parametric amplifier with chirped mirrors or with two prisms. The measurements shown in Fig. 2d and in Supplementary Fig.1 have been performed at room temperature with pump fluences corresponding to 1.3 and 2.8 mJ cm^{-2} for above-gap or sub-gap pump pulses, respectively. The higher noise conditions of this set of measurements do not allow to investigate the linear response regime for the system, while the high intensities in both pump and probe pulses (≥ 0.2 mJ cm^{-2}) are responsible for unavoidable artefacts in the transient responses. For these reasons, we limited the KK-based analysis of the optical conductivity to the long pulse measurements, which are safely in the linear response limit.

Furthermore, we notice that the observed thermalization times are different for the two excitation schemes with ~ 100 and sub-20 fs pulses. This might be partially due to the fact that excitations produced by light pulses at certain wavelengths undergo a state-specific thermalization pathway. The longer times detected with ~ 100 fs pulses partially support this scenario. However, we stress that the two excitation schemes differ not only in terms of the excited states involved, but also regarding the pulse energies used, and this can affect the observed timescales. Further studies are needed to clarify this issue. Nonetheless, it is remarkable that both results confirm a pulse-width-limited non-thermal reaction of the bosonic field for $E_{pump} < \Delta$.

Finally, we can exclude the slow rise time measured for $E_{pump} > \Delta$ to be related to diffusion of the photo-excitation energy along the surface normal. In such case, one would expect slower rise times for shorter probe wavelengths. This effect is not observed in our experiments (see Supplementary Fig. 3).

Thermal effects. The optical response of the CTP as a function of pump–probe delay is reported in Fig. 2c for $E_{pump} > \Delta$ (solid blue curve) and $E_{pump} < \Delta$ (solid red curve), respectively. The transient conductivity probed at 2.3 eV for $E_{pump} = 0.95$ eV is properly normalized by the factor N, calculated as follows. The pump energy density absorbed by the sample and detected by a single-colour probe with energy E_{probe} is equal to $\frac{\Phi(E_{pump})}{x(E_{probe})} \cdot \left[1 - R(E_{pump}) \right] \cdot \left[1 - e^{-x(E_{probe})/x(E_{pump})} \right]$, where $\Phi(E)$ is the fluence, $R(E)$ is the reflectivity and $x(E)$ is the penetration depth for photons with energy E. Considering the bandwidth of the pump pulse and averaging over the probe energy range ΔE_{probe}, the effective energy density is

$$Q(E_{pump}; E_{probe}) = \frac{1}{\Delta E_{probe}} \iint \frac{\Phi(E_{pump})}{x(E_{probe})} \cdot \left[1 - R(E_{pump}) \right] \cdot \left[1 - e^{-x(E_{probe})/x(E_{pump})} \right]$$

$dE_{probe} dE_{pump}$. Making use of the reflectivity and the penetration depth as determined from the ellipsometry data (see Fig. 1 and Supplementary Fig. 4b), the ratio $N = \frac{Q(E_{pump}=3.1eV;1.9eV<E_{probe}<2.5eV)}{Q(E_{pump}=0.95eV;1.9eV<E_{probe}<2.5eV)}$ turns out to be ~ 14 at $T = 130$ K, which is the normalization factor used in Fig. 2c.

The absorbed pump energy density can be directly related to the increase of the sample temperature ΔT detected by the probe pulses. In particular, $\Delta T = \frac{Q(E_{pump};E_{probe})}{\delta \cdot C}$ where δ denotes the mass density and C the specific heat. Being $C \approx 0.2$J/K $\cdot$ g at $T = 130$ K (ref. 41) and $\delta \approx 7$g cm^{-3}, the expected temperature reached by the sample when all the degrees of freedom thermalize is $T + \Delta T \approx 139$ K. Thus, we expect that the laser-driven transient response at long pump–probe delays should be comparable to the difference between the equilibrium optical quantities measured at 130 K and at 139 K. A comparison among the off-equilibrium $\Delta \sigma_1(\omega, \tau = 5$ ps) and the difference between the

equilibrium conductivities $\sigma_1(T = 139\,K)$ and $\sigma_1(T = 130\,K)$ reveals a very good agreement, see the black dashed curves in Fig. 1c and in Fig. 3b and Supplementary Fig. 4. The dashed line in Fig. 1c is obtained by a linear interpolation of the data in ref. 6.

Data analysis. To extract the time-dependent optical quantities such as the dielectric function (ε) or the optical conductivity (σ) out of pump–probe reflectivity $\Delta R(\omega, \tau)/R(\omega) = R(\omega, \tau)/R(\omega) - 1$, we proceed as follows. We obtain the equilibrium reflectivity $R(\omega)$ from the measured ellipsometry data between 1 and 3.2 eV and from the literature outside of this range[6,42]. We perform a Drude–Lorentz fit[43,44] of the broadband equilibrium reflectivity over a wide energy range, from a few meV up to several tens of eV. We calculate the real and imaginary parts of the equilibrium dielectric function, $\varepsilon_1(\omega)$ and $\varepsilon_2(\omega)$, in the entire energy range through the KK relations[45].

The time-resolved $\Delta R(\omega, \tau)/R(\omega)$ is measured in the 1.5–3.1 eV energy range. To obtain the time-domain changes of the optical functions, we consider only the regime where the variations of the reflectivity $\Delta R(\omega, \tau)$ (up to 10^{-2} as shown in Supplementary Fig. 5) is linear with the pump fluence. We make the assumption that the variations of the pump-perturbed reflectivity outside the probed energy range are either small or distant on the energy scale so that they do not affect significantly the optical response in the probed range of 1.5–3.1 eV. Starting from these assumptions, both the measured reflectivity $\Delta R(\omega, \tau)/R(\omega)$ and the equilibrium reflectivity $R(\omega)$ are known over a broad energy range, that is, from a few meV up to several tens of eV. Hence, the time evolution of the optical quantities such as $\varepsilon_1(\omega, \tau)$ and $\varepsilon_2(\omega, \tau)$ can be obtained by the KK transformations. The results of this analysis performed on the data measured at 130 K are reported in Fig. 2. The photo-induced variation of the real part of the optical conductivity $\Delta \sigma_1(\omega, \tau) = \sigma_1(\omega, \tau)$-$\sigma_1(\omega)$ is shown for $E_{pump} = 3.1$ eV (Fig. 2a) and $E_{pump} = 0.95$ eV (Fig. 2b). We include for clarity the reflectivity data in Supplementary Fig. 5 and Supplementary Fig. 6. We emphasize that our analysis is consistent because the same normalization factor is used in Fig. 2c (that displays $\Delta \sigma_1$) and in Supplementary Fig. 7 (where $\Delta R/R$ is shown).

We implement a transfer-matrix method to correct the effect of the mismatch between the penetration depths of the pump and the probe pulses on the amplitude of the time-domain signal. We assume a pump-perturbed exponentially graded index of refraction at the material surface by means of multiple planes, each with a thickness of 1 nm. The total reflection is calculated exploiting the continuity conditions for the electric fields across these boundaries. Further details can be found in refs 46,47 Being the penetration depth at ~ 0.95 eV larger than the one of any probe in the 1.5–3 eV range, one expects significant corrections only for $E_{pump} \sim 3.1$ eV. The detailed numerical analysis confirms this simple picture. This is made evident in Supplementary Figs 8 and 9 for pump–probe delay time $\tau = 0.1$ ps averaged over ± 0.1 ps. The $\Delta R(\omega, \tau)/R(\omega)$ obtained in this way for $E_{pump} \sim 3.1$ eV has been used as starting point for the KK analysis described in the previous paragraph. The corrections to the transient reflectivity are obtained as summarized in Supplementary Fig. 9.

HHH details. The time-dependent potential vector adopted is[48]

$$A = A_0 e^{-\frac{(\tau - \tau_0)^2}{\tau_{pump}^2}} \cos\big(\omega_{pump}(\tau - \tau_0)\big), \qquad (4)$$

and the optical conductivity at time τ, after the end of the pump, is given by[49,50]

$$\sigma(\omega, \tau) = \frac{1}{M\omega} \Im \int_0^\infty i e^{i(\omega + i\eta)t} \langle \Psi(\tau) \,|\, [j(t), j(0)] \,|\, \Psi(\tau)\rangle dt. \qquad (5)$$

Here $|\Psi(\tau)\rangle = T e^{-i \int_0^\tau H(\tau_1) d\tau_1} |\Psi(\tau = 0)\rangle$, T is the time-ordering operator, $j(t)$ is the current operator in the Heisenberg representation along one of the lattice axes, η is a broadening factor taking into account additional dissipative processes and M is the number of lattice sites. The $|\Psi(\tau)\rangle$ state is obtained through the Lanczos time-propagation method[51]. In the following, we use periodic boundary conditions on two-dimensional lattices[52] with $M = 8$.

The local nature of the interactions involved in the HHH allows us to extract the relevant physics of the model (at least at a qualitative level) also by using a small lattice, which, on the other hand, reproduces most of the discrete symmetries of the square lattice, and contains the relevant momenta: $\left(\pm \frac{\pi}{2}, \pm \frac{\pi}{2}\right)$, $(\pi, 0)$, $(0, \pi)$, $(0, 0)$ and (π, π). It is worth noting that the chosen lattice does not frustrate the antiferromagnetic ground state[52]. These important properties are a consequence of the 'special' eight site lattice introduced first in ref. 53.

Within the used approach, the charge and spin degrees of freedom are exactly treated: all the possible states are considered in subspaces with a well-defined value of the z component of the total spin. The real bottleneck comes from the infinite dimensional Hilbert space required by the boson excitations. To solve this problem, we use a generalization of the method recently introduced in the Holstein[35] and Su-Schrieffer-Heeger model[34]: the double-boson approach. It is based on a smart truncation of the boson Hilbert space including two distinct sets of states. In the first set of basis elements, there are up to four bosons distributed in all possible ways. Of course, in this way the scattering processes among charge carriers and boson excitations up to four quanta are treated exactly also in **q** space. This set is able to recover the self-consistent Born approximation and goes beyond it, including vertex corrections. In the other set of states, local excitations of any strength (up to 15 boson

excitations per site) are distributed at most on two sites, which are located at arbitrary positions with respect to the charge carriers. The double-boson approach used in this study is based on the idea that the physical properties for any value of the electron–boson interaction can be described by diagonalizing the Hamiltonian in the bosonic Hilbert subspace generated by the two sets of states introduced above (excluding obvious double counting).

The pump pulses adopted in the model have slightly different temporal and energetic content with respect to the ones used in the experiments. This is mainly due to finite size effects, explained as follows.

Concerning the frequency of the pump pulses, we have chosen $E_{pump} = 1.9$ eV and $E_{pump} = 3.2$ eV for sub-gap and above-gap pump pulses, respectively. In particular, for the sub-gap case, we were forced to use a larger value than that one used in the experiments for two reasons. First, solving the HHH on a small lattice implies few sparse discrete eigenstates at low energy, resulting in the lowest optical transition at ~ 1.9 eV that is absent in the bare Hubbard model. Second, our model does not include the free charge in excess present in the experimental sample. In addition to this, we highlight that the model is provided at $T = 0$ K while it is well known that the CT gap in La_2CuO_4 shifts to higher energies on cooling[30–32].

Moreover, the theory adopted ~ 40 fs long pulses, while the experiments made use of ~ 100 fs pulses. In the case of a small lattice, as the one used in our model, the allowed eigenvalues are restricted to a discrete set with a finite separation between them. However, due to the uncertainty principle, the more the duration of the pump pulse increases, the narrower is the energy. Hence, our model cannot use pump pulses exceeding ~ 40 fs, as the energy uncertainty of the pump pulses would be smaller than the typical distance between two adjacent eigenvalues. In this condition, a light pulse would excite only one eigenstate of the Hamiltonian resulting in a state not evolving in time.

Nonetheless, we stress that this limit of the theory is intrinsic in the finite size of our lattice and a comparison between experiment and theory is possible as the experimental pulse will always excite a superposition of eigenstates of the system. The linearity with the pump intensity of the observed response for both experiment and theory further consolidates the validity of the comparison.

In the main text, we focused our attention on the properties of $|\phi(\tau)\rangle$, the photo-excited component of the wave-function $|\Psi(\tau)\rangle$. It is defined in terms of the wave function at time τ and $|\Psi_{GS}\rangle$, the normalized ground state of the HHH in absence of the electromagnetic field: $|\Psi(\tau)\rangle = \sqrt{1 - |b(\tau)|^2} |\Psi_{GS}\rangle + b(\tau)|\phi(\tau)\rangle$.

The expectation value of any observable A, measured with respect to the value in the ground state wavefunction, is: $\langle \Psi(\tau)|A|\Psi(\tau)\rangle - \langle \Psi_{GS}|A|\Psi_{GS}\rangle = |b(\tau)|^2$ $(\langle\phi(\tau)|A|\phi(\tau)\rangle - \langle\Psi_{GS}|A|\Psi_{GS}\rangle) + \Delta A$, where ΔA is proportional to the matrix element of the observable between the ground state and photo-excited component. As the last term is negligible (we checked it for all the quantities investigated in the paper), the ratio between the values of any fixed physical quantity, measured in the wavefunctions corresponding to above- and sub-gap pulses, is always proportional to the ratio between the weights associated to the photo-excited components of the two wavefunctions. This ratio is about 10 for the chosen parameter values and delay larger than the pump pulse duration. Taking into account the smaller excitation fluence for the sub-gap case in the experimental data, we find a good agreement between theory and experiments.

Finally, we address the role of the pump pulse duration in the Hubbard–Holstein calculations (Supplementary Fig. 10). In general, one expects that for longer pump pulses the non-thermal part of the dynamical response of a system to be diminished in favour of the thermal dynamics. As the observed ultrafast shift of the transient optical conductivity is related to the non-thermal response in $La_2CuO_{4+\delta}$ for $E_{pump} < \Delta$, one expects that the shorter the pump pulse, the larger the shift in $\Delta \sigma_1(\omega, \tau)$. This is confirmed by the calculations displayed in Supplementary Fig. 10 corresponding to ~ 20 fs long pump pulses, and by the experiments shown in Supplementary Fig. 1. We stress that all the calculations predict an ultrafast transient negative change of $\Delta \sigma_1(\omega, \tau)$ for $E_{pump} < \Delta$, that evolves towards the thermal response at long pump–probe delays. This is confirmed by both ~ 10 and ~ 100 fs resolution experiments.

References

1. Imada, M., Fujimori, A. & Tokura, Y. Metal-insulator transitions. *Rev. Mod. Phys.* **70**, 1039 (1998).
2. Tokura, Y. Correlated-electron physics in transition-metal oxides. *Phys. Today* **56**, 50 (2003).
3. Ahn, C. H. *et al.* Electrostatic modification of novel materials. *Rev. Mod. Phys.* **78**, 1185 (2006).
4. Salamon, M. B. & Jaime, M. The physics of manganites: Structure and transport. *Rev. Mod. Phys.* **73**, 583 (2001).
5. Tokura, Y. *et al.* Cu-O network dependence of optical charge-transfer gaps and spin-pair excitations in single-CuO₂-layer compounds. *Phys. Rev. B* **41**, 11657 (1990).
6. Uchida, S. *et al.* Optical spectra of La₂SrCuO₄. Effect of carrier doping on the electronic structure of the CuO₂ plane. *Phys. Rev. B* **43**, 7942–7954 (1991).
7. Perkins, J. D. *et al.* Mid-infrared optical absorption in undoped lamellar copper oxides. *Phys. Rev. B* **71**, 1621–1624 (1993).
8. Perkins, J. D. *et al.* Infrared optical excitations in La₂NiO₄. *Phys. Rev. B* **52**, R9863–R9866 (1995).

9. Perkins, J. D. *et al.* Midinfrared optical excitations in undoped lamellar copper oxides. *Phys. Rev. B* **58**, 9390–9401 (1998).

10. Mishchenko, A. S. *et al.* Charge dynamics of doped holes in high Tc superconductors: a clue from optical conductivity. *Phys. Rev. Lett.* **100**, 166401 (2008).

11. Lupi, S. *et al.* Far-infrared absorption and the metal-to-insulator transition in hole-doped cuprates. *Phys. Rev. Lett.* **102**, 206409 (2009).

12. Nicoletti, D. *et al.* An extended infrared study of the p,T phase diagram of the p-doped Cu–O plane. *New J. Phys.* **13**, 123009 (2011).

13. De Filippis, G. *et al.* Quantum dynamics of the Hubbard-Holstein model in equilibrium and nonequilibrium: application to pump-probe phenomena. *Phys. Rev. Lett.* **109**, 176402 (2012).

14. Basov, D. N. *et al.* Electrodynamics of correlated electron materials. *Rev. Mod. Phys.* **83**, 471 (2011).

15. Norman, M. R. & Pepin, C. The electronic nature of high temperature cuprate superconductors. *Rep. Prog. Phys.* **66**, 1547 (2003).

16. Han, J. E., Gunnarsson, O. & Crespi, V. H. Strong superconductivity with local Jahn-Teller phonons in C60 solids. *Phys. Rev. Lett.* **90**, 167006 (2003).

17. Capone, M., Fabrizio, M., Castellani, C. & Tosatti, E. Strongly correlated superconductivity. *Science* **296**, 2364–2366 (2002).

18. Bonča, J., Maekawa, S., Tohyama, T. & Prelovšek, P. Spectral properties of a hole coupled to optical phonons in the generalized *t-J* model. *Phys. Rev. B* **77**, 054519 (2008).

19. Cataudella, V., De Filippis, G., Mishchenko, A. S. & Nagaosa, N. Temperature dependence of the angle resolved photoemission spectra in the undoped cuprates: self-consistent approach to the *t-J* Holstein model. *Phys. Rev. Lett.* **99**, 226402 (2007).

20. Rösch, O. & Gunnarsson, O. Apparent electron-phonon interaction in strongly correlated systems. *Phys. Rev. Lett.* **93**, 237001 (2004).

21. Dodge, S., Schumacher, A. B., Miller, L. L. & Chemlaet, D. S. Optically induced softening of the charge-transfer gap in $Sr_2CuO_2Cl_2$. Preprint at http://arxiv.org/abs/0910.5048 (2009).

22. Sangiovanni, G., Capone, M., Castellani, C. & Grilli, M. Electron-phonon interaction close to a Mott transition. *Phys. Rev. Lett.* **94**, 026401 (2005).

23. Carbotte, J. P., Timusk, T. & Hwang, J. Bosons in high-temperature superconductors: an experimental survey. *Rep. Prog. Phys.* **74**, 066501 (2011).

24. Johnston, S. *et al.* Systematic study of electron-phonon coupling to oxygen modes across the cuprates. *Phys. Rev. B* **82**, 064513 (2010).

25. Johnston, S. *et al.* Material and doping dependence of the nodal and antinodal dispersion renormalizations in single- and multilayer cuprates. *Adv. Condens. Matter Phys.* **2010**, 968304 (2010).

26. Falck, J. P., Kastner, M. A., Levy, A. & Birgenau, R. J. Charge-transfer spectrum and its temperature dependence in La_2CuO_4. *Phys. Rev. Lett.* **69**, 1109–1112 (1992).

27. Keimer, B. *et al.* Néel transition and sublattice magnetization of pure and doped La_2CuO_4. *Phys. Rev. B* **45**, 7430 (1992).

28. Mysyrowicz, A. *et al.* 'Dressed excitons' in a multiple-quantum-well structure: evidence for an optical stark effect with femtosecond response time. *Phys. Rev. Lett.* **56**, 2748 (1986).

29. Becker, P. C., Fork, R. L., Brito Cruz, C. H., Gordon, J. P. & Shank, C. V. Optical stark effect in organic dyes probed with optical pulses of 6-fs duration. *Phys. Rev. Lett.* **60**, 2462 (1988).

30. Okamoto, H. *et al.* Ultrafast charge dynamics in photoexcited Nd_2CuO_4 and La2CuO4 cuprate compounds investigated by femtosecond absorption spectroscopy. *Phys. Rev. B* **82**, 060513(R) (2010).

31. Okamoto, H. *et al.* Photoinduced transition from Mott insulator to metal in the undoped cuprates Nd_2CuO_4 and La_2CuO_4. *Phys. Rev. B* **83**, 125102 (2011).

32. Matsuda, K. *et al.* Femtosecond spectroscopic studies of the ultrafast relaxation process in the charge-transfer state of insulating cuprates. *Phys. Rev. B* **50**, 4097–4101 (1994).

33. Lövenich, R. *et al.* Evidence of phonon-mediated coupling between charge transfer and ligand field excitons in $Sr_2CuO_2Cl_2$. *Phys. Rev. B* **63**, 235104 (2001).

34. Marchand, D. J. J. *et al.* Sharp transition for single polarons in the one-dimensional Su-Schrieffer-Heeger model. *Phys. Rev. Lett.* **105**, 266605 (2010).

35. De Filippis, G., Cataudella, V., Mishchenko, A. S. & Nagaosa, N. Optical conductivity of polarons: double phonon cloudconcept verified by diagrammatic Monte Carlo simulations. *Phys. Rev. B* **85**, 94302 (2012).

36. Mishchenko, A. S. & Nagaosa, N. Electron-phonon coupling and a polaron in the t-J model: from the weak to the strong coupling regime. *Phys. Rev. Lett.* **93**, 36402 (2004).

37. De Filippis, G., Cataudella, V., Mishchenko, A. S. & Nagaosa, N. Nonlocal composite spin-lattice polarons in high temperature superconductors. *Phys. Rev. Lett.* **99**, 146405 (2007).

38. Fausti, D. *et al.* Light-induced superconductivity in a stripe-ordered cuprate. *Science* **331**, 189–191 (2011).

39. Kaiser, S. *et al.* Optically induced coherent transport far above Tc in underdoped $YBa_2Cu_3O_{6+\delta}$. *Phys. Rev. B* **89**, 184516 (2014).

40. Boyd, R. W. *Nonlinear Optics* (Academic Press, Third edition, 2007).

41. Sun, K. *et al.* Heat capacity of single-crystal La_2CuO_4 and polycrystalline $La_{1-x}Sr_xCuO_4$ ($0 \leq x \leq 0.20$) from 110 to 600 K. *Phys. Rev. B* **43**, 239 (1991).

42. McBride, J. R., Miller, L. R. & Weber, W. H. Ellipsometric study of the charge-transfer excitation in single-crystal La_2CuO_4. *Phys. Rev. B* **49**, 12224–12229 (1994).

43. Novelli, F. *et al.* Ultrafast optical spectroscopy of the lowest energy excitations in the Mott insulator compound YVO_3: evidence for Hubbard-type excitons. *Phys. Rev. B* **86**, 165135 (2012).

44. Reul, J. *et al.* Temperature-dependent optical conductivity of layered $LaSrFeO_4$. *Phys. Rev. B* **87**, 205142 (2013).

45. Wooten, F. *Optical Properties Of Solids* (Academic press, 1972).

46. Dal Conte, S. *et al.* Disentangling the electronic and phononic glue in a high-Tc superconductor. *Science* **30**, 335 (2012).

47. Cilento, F. *Non-Equilibrium Phase Diagram Of $Bi_2Sr_2Y_{0.08}Ca_{0.92}Cu_2O_{8+\delta}$ Cuprate Superconductors Revealed By Ultrafast Optical Spectroscopy*. Ph.D. thesis, Univ. Trieste (2011).

48. Matsueda, H., Sota, S., Tohyama, T. & Maekawa, S. Relaxation dynamics of photocarriers in one-dimensional Mott insulators coupled to phonons. *J. Phys. Soc. Jpn* **81**, 013701 (2012).

49. Fetter, A. L. & Walecka, J. D. *Quantum Theory of Many Particle Systems* (McGraw-Hill S, 1971).

50. Balzer, M., Gdaniec, N. & Potthoff, M. Krylov-space approach to the equilibrium and nonequilibrium single-particle Green's function. *J. Phys. Condens. Matter* **24**, 035603 (2012).

51. Park, T. J. & Light, J. C. Unitary quantum time evolution by iterative Lanczos reduction. *J. Chem. Phys* **85**, 5870 (1986).

52. Dagotto, E., Joynt, R., Moreo, A., Bacci, S. & Gagliano, E. Strongly correlated electronic systems with one hole: dynamical properties. *Phys. Rev. B* **41**, 9049 (1990).

53. Oitmaa, J. & Betts, D. D. The ground state of two quantum models of magnetism. *Can. J. Phys.* **56**, 897 (1978).

Author contributions

F.N., D.F. and E.S. performed the broadband probe experiments. F.C. and D.F. developed the white-light optical setup. F.N., M.E., S.C. and G.C. performed the high-temporal-resolution measurements. F.N., D.F. and F.P. analysed the data and coordinated the project. M.G. and I.V. performed and analysed magnetic and broadband ellipsometry measurements at several temperatures of interest. G.F., V.C., N.N. and A.M. developed the theoretical framework. G.F. and V.C. performed the calculations. F.N., D.F., G.F. and V.C. wrote the manuscript after discussing with all the co-authors. S.W., C.G., A.A. and M.C. have given particularly important comments. A.P. performed equilibrium reflectivity measurements in the visible range. D.P. and S.W. made and furnished high-quality oriented and polished single crystals.

Additional information

Supplementary Information accompanies this paper at http://www.nature.com/naturecommunications

Competing financial interests: The authors declare no competing financial interests.

Reprints and permission information is available online at http://npg.nature.com/reprintsandpermissions/

How to cite this article: Novelli, F. *et al.* Witnessing the formation and relaxation of dressed quasi-particles in a strongly correlated electron system. *Nat. Commun.* 5:5112 doi: 10.1038/ncomms6112 (2014).